IEPC-93-172

Test-to-Failure of a Two-Grid, 30-cm-dia. Ion Accelerator System

John R. Brophy*, Jal))cs li. I'olk**, al)d I.c\vis C.l'less+
Jet Propulsion Laboratory
California Institute of Technology
Pasadena, California

To determine the failure mechanism and erosion characteristics of an ion accelerator **system due to** erosion **by** char~c-exchange ions a test **was performed** in which **a 30-cm-diameter, 2-grid** ion **accelerator system was tested** to failure. **The** erosion **rate** of the accelerator grid was artificially **enhanced by performing the test** at **a vacuum chamber pressure of** 3. **5x10^{-3} Pa** and **by operating the engine with** an **accelerator grid voltage of -500 V. The accelerator system failed when material that** was **sputter deposited on to the screen** grid from **the accelerator** grid formed a **flake which shorted the grids** together. 1'0s1 test inspection indicated that the accelerator grid was also close **to** structural failure at **the time** his **short** occurred. Analyses indicate the **grid** may have lost as much as **58 g at the** time of failure. **Operation** at the relatively high vacuum chamber pressure used in this test **appears to have broadened** the radial mass loss **profile** relative **to the** radial ion **beam** current profile. 1'0 a **large** extent, the charge-cxchangc erosion appears **to** remain **within** the **"pits & grooves" pattern that is established in short term tests. The erosion characteristics observed in this** test, **however, imply** significantly **shorter** accelerator grid **life times** than typically slated in **the** literature. Finally, the **test** suggests that **structural** failure is probably not **the** most likely first failure mechanism for the accelerator grid.

introduction

The life-limiting component for state-of-lhc-at 1, xenon-fed, gridded ion engines is currently believed to bc the accelerator grid of the ion accelerator system. The conventional accelerator system under development by NASA **[Patterson-1993]** for the 30-cm diameter ion engine consists of two closely-spaced, dished molybdenum electrodes. The upstream electrode, called the screen grid, is typically 0.38 mm thick and contains approximately 15,000 circular holes, 1.9 mm in diameter, resulting in a physical open area fraction of approximately 0.67. The accelerator grid, which is the downstream grid as indicated in Fig. 1, may bc up to 60% thicker than the screen grid. It is typically fabricated with holes that arc smaller in diameter than those in the screen grid, resulting in a lower open area fraction. The accelerator grid is maintained several hundred volts negative of neutralizer common to both focus the ion beamlets through the accclc.rater system and to prevent electrons emitted by the neutralizer cathode from "backstreaming" to the positive high voltage engine.

The useful life of the accelerator grid is limited by sputter erosion of the grid materially charge-exchange ions. These ions arc created by charge-cxchangc collisions between positive ions accelerated from the thruster and neutral propellant atoms in the inter-giid region or outside of the engine. The collisions result in fast moving neutral atoms and slow moving ions. Depending on where. these collisions take place these slow moving positive ions may bc attracted back to the negative accelerator grid where they will strike it with a maximum energy in electron volts equal to the negative potential applied to the grid.

The neutral propellant atoms which participate in these charge-cxchang,c collisions may originate as propellant which escaped from the engine unionized or they may bc part of the background gas in the vacuum test chamber due to the finite pumping speed of the facility. In space the only atoms present will bc those which escape from the engine unionized (either through the grid apertures or from the neutralizer cathode). The effect of a non-zero background pressure in vacuum chamber tests can artificially shorten the useful li fc of the accelerator grid bya substantial amount by increasing the production rate of charge-cxchangc ions.

Although it is believed that accelerator grid erosion by charge-exchange ions is the life-limiting mechanism for xenon-fed ion engines, exactly how the erosion results in grid failure is not known. In the 13 years of development testing of l-arc-gas-fed ion engines by NASA, the longest test

*Supervisor, Advanced Propulsion Technology Group
** Member of the Technical Staff, Advanced Propulsion Technology Group
+Member of the Technical Staff, Electric Power Systems Section.

of an ion engine operated on xenon with a two-grid accelerator system is only 900 hews [Patterson-1990].

The dearth of long term test data, together with projected mission-dictated engine life requirements of 10,OO(I hours or more, have necessitated the extrapolation of short term test data by at least an order of magnitude in order to estimate the useful engine life. This procedure is inherently inaccurate and estimates of accelerator grid life can easily vary by more than a factor of two depending on the assumptions used to make this lengthy extrapolation. For example, the accelerator grid life is estimated in Ref. [Patterson-1990] to be greater than 11 ,S00 hours for the NASA 30-cm engine operated on xenon io space a! 5.5 kW. Using different assumptions we deterministically calculate the time to structural failure of the accelerator grid to be only 4600 hoots in space. This difference in estimated grid life arises primarily from the use of different assumptions regarding how to extrapolate the grid erosion pattern 10 structural failure.

To determine the Iong-term behavior of the accelerator grid erosion pattern and to identify the failure mechanism of the accelerator grid doc to charge-c.xchangc ion erosion a test was conducted in which a 30-cm dia. ion engine was intentionally operated until the accelerator grid failed. The results from this test-to-failure also formed the basis for the erosion model used in the probabilistic assessment of the accelerator grid life described in Ref. [Polk-1993]

In this lcsl-to-failure the accelerator grid erosion rate was artificially increased by performing the test at an elevated vacuum chamber pressure of 3.9×10^{-3} Pa (3×10^{-5} ton) and by operating with an accelerator grid voltage of -S00 volts. Krypton was used instead of xenon in order to reduce the cost of performing the test,

Accelerator Grid Erosion Models

A simple model was used in Ref. [Patterson-1990] to extrapolate the accelerator grid erosion observed at the end of 960 boors of operation in order 10 predict the time to structural failure of the grid. Charge-exchange erosion normally results in a "pits & grooves" pattern 011 the downstream face of the accelerator grid as shown in Fig. 2. The pits are formed at the locations which are equidistant from the centers of any three grid apertures. The groves arc straight channels which connect the pits along the grid webbing. In the locations where erosion occurs, the erosion rate is the highest in the pits and lowest midway between the pits along the grooves. Very little erosion appears to take place outside of this "pits & grooves" pattern.

in the mode] of Ref. [Patterson-1990] the minimum groove erosion depth (i.e., the erosion depth in the groove. at the midpoint between the pits) was measured at the center region of the accelerator grid. An erosion rate was then calculated by dividing this erosion depth (which was 76 microns) by the total thruster operating time at 5.5 kW of 906 hours to get 84 microns/khr. Assuming this rate is constant with time, the model predicts a time to structural failure for the 360-micron thick grid used in this test of 4300 hours (as stated in [Patterson-1990]) under the conditions of the test. The predicted lifetime of 4300 hours under the ground test conditions is a factor of 4.7 times longer than the actual test duration at 5.5 kW. Reference [Patterson-1990] also stated that 17.? g of material had been removed from the accelerator grid as a result of erosion by charge-exchange ions over the course of the 906 hours of operation at 5.5 kW and an additional 51 boors at a variety of throttled conditions resulting in an average erosion rate of 18.0 g/khr. Assuming this mass loss rate is constant with time and multiplying it by 4.3 khr (the calculated time to structural failure) suggests that when the grid fails it will have lost approximately 77 g of material.

The key assumption in this model is that the linear erosion rate in the g roove midway between the pits is constant with time. The key predictions arc that the grid will fail structurally at 4300 hours and that when it fails it will have lost 77 g. The assumption of a constant linear groove erosion rate is the simplest assumption to make, but it may lead to a substantial over estimation of the accelerator grid life. The accelerator grid test-to-failorc described in this paper provides sufficient information to test the validity of this model by examining both the assumption of constant linear erosion rate and the prediction of the total mass loss at struct oral failure.

Proposed Accelerator Grid Erosion Model

An alternative accelerator grid erosion model is based on the assumption that the accelerator grid erosion takes place only in the "pits & grooves" regions even when the grid is close to structural failure. It also assumes that the mass removal rate from the grid is constant with time. In this model, the time to structural failure of the grid is determined by the time it takes to remove all of the grid mass within the pits & grooves pattern al the location on the grid where the ion current density is the highest, To determine this mass we start by calculating the total mass of the accelerator grid webbing, m_a,

$$m_a = \pi r_b^2 t_a \rho (1 - \phi_a), \qquad (1)$$

where r_b is the radios of the active grid area, t_a is the grid thickness, p is the density of the grid material and φ_a is the physical open area fraction of the grid when new. The mass of the grid webbing which would be eroded if the pits & grooves pattern were to erode completely through the grid over the entire active area is given by

$$m_e = \pi r_b^2 t_a \rho (1-\phi_a)\alpha, \qquad (2)$$

where α is the fraction of the grid webbing area covered by the pits & grooves erosion pattern as shown in Fig. 2. The distribution of mass removal, however, is not uniform over the grid because the distribution of ion current to the grid is non-uniform, being typically peaked on the centerline of the thruster. Consequently, the accelerator grid will fail structurally when the total mass removed is less than m_e. Defining the accelerator grid current flatness parameter, f_a, as the ratio of peak to average accelerator grid current density, then structural failure of the accelerator grid will occur when the following amount of grid mass is removed,

$$m_{fail} = \pi r_b^2 t_a \rho (1-\phi_a)\alpha f_a \qquad (3)$$

This equation implies that the accelerator grid fails structurally when the pits & grooves erosion pattern erodes completely through the grid at the location of highest ion current density.

For the molybdenum grid of Ref. [Patterson-1990], r_b = 285 mm, φ_a = 0.24. In addition, a value of α = 0.4 is estimated for this grid from photographs provided by NASA LeRC [Rawlin-1993]. Assuming f_a is equal 10 the beam flatness parameter. which is estimated to be 0.S, results in the estimation that accclc.rater grid failure will occur when m_{fail} = 38 g. This is considerably less than the 77 g estimated above. For the. operating conditions of Ref. [Patterson-1990] the accelerator grid erosion rate was 18,0 g/khr. Thus, this model predicts that the accelerator grid would have failed in approximately 2,1OO hours under the test conditions.

Adjusting the material removal rate for conditions expected in space by reducing the accelerator grid impingement current to 0.25% of the beam current results in a predicted accelerator grid life in space of 4600 hours. This assumes that the both the eroded area fraction, α, and the accelerator grid current flatness parameter, f_a, arc the same in space as they arc in the ground test, and as stated earlier, it also assumes that the rate at which mass is removed from the accelerator grid is a constant.

To test the validity of this model the accelerator grid tcs(-to-failure was executed. Onc of the primary objectives of this test was to determine the accelerator grid erosion pattern as the grid approached structural failure.

Apparatus and Procedure

Vacuum Test Facility

The accelerator grid test-to-failure was performed in a 2.4-III diameter by 5-IN long stainless steel vacuum chamber. The chamber is equipped with two 0.81-m dia. oil diffusion pumps and one 1.2-m dia, oil diffusion pump. Laboratory power supplies were used for all engine start-up and operating functions. Propellant flow rate control was accomplished using a precision pressure regulator and three micrometer valves (one each for the main flow into the discharge chamber, the flow through the discharge chamber cathode, and the flow through the neutralizer cathode). The micrometer valves were set to give the desire.d flow rates at the regulated pressure and then functioned as fixed flow restrictors throughout the test. The vacuum facility and ion engine operation were monitored by computer and with the capability to safely shutdown the engine or the engine and the facility ifa fault is detected. The primary cam target was a wedged shaped structure covered in grafoil ~grafoil-1993] in order to reduce the amount of material back sputtered to the engine. The back sputtered material was recorded by glass slides placed next to the thruster during the lest-to-failure.

Thruster Modifications

The test-to-failure was performed using a 30-cm diameter, J-series **[J-Series Reference]** thruster which had been substantially modified to first operate on inert gas rather than mercury, and subsequently to make it functionally closer to a ring-cusp magnetic field configuration. The modified configuration is compared to the J-Series thruster in Fig. 3. An Alnico-5 ring magnet was added to the back plate of the thruster. The cathode pole piece was modified to eliminate the baffle and baffle support structure., A multiorifice cathode [Annual Report-1990] was used for the main discharge chamber cathode. The cylindrical anode was shortened by removing approximately 30 m m from the downstream end. A second anode electrode was added to the upstream end of the discharge chamber. This washer-shaped electrode was positioned just downstream of the thruster back-plate and covered the ring magnet placed there. Finally, a ring of Alnico-8 magnets was added just outside the anode pole. piece as indicated in the figure. This ring of magnets, along with the anode pole piece were maintained at cathode potential throughout the test.

Accelerator System

The accelerator system used in the lest-to-failu~c was from one of the 30-cm, J-Series thrusters built in the late 1970s. The grids arc nominally 0.381 mm thick. The screen grid and accelerator grid apertures arc 1.91 and 1,14 mm in diameter respectively. The accelerator system had an unknown amount of operating time on it prior to this test. The initial conditions of the accelerator grid are shown in Fig. 4. The normal pits & grooves pattern is visible in all three of these photographs. At mid-radius the. grooves appear as little more than a discoloration of the surface. The pits at the center of the grid were estimated by inspection to be a only small fraction of the grid thickness. The exact amount of material removed from the accelerator grid as a result of testing performed prior to the tcs(-to-failure is unknown.

Results and Discussion

Operating Characteristics

The perveance characteristic for this thruster configuration is given in Fig. 5 for operation at a beam current of 2.8 A with krypton propellant, The perveance limit is approximately 1100 V, which is consistent with a beam flatness parameter of 0.55 (for a grid gap of 0.61 mm). The Icsl-to-failure was performed with an accelerator grid voltage of -500 V. The large negative voltage was used to artificially accelerate the accelerator grid erosion. The screen grid voltage was maintained at 1050 V through out most of the test resulting in a total voltage of 1550 V. This is well away from the perveance limit of the accelerator system and was done to minimize direct ion impingement on the accelerator grid.

The operating parameters as a function of time are given in Fig. 6 for the test-to-failmc. The nominal operating conditions are summarized in '1'able 1. Significantly, there was no long term variation in the average value of the accelerator grid current over the course of this test as indicated in Fig. 6. Of equal significance, these data indicate that there appeared tobc no substantial changes in any of the key performance parameters: beam current, discharge voltage, propellant flow rates, and coupling voltage. This is remarkable in view of the substantial amount of erosion sustained by the accelerator grid as will be shown later.

The vacuum chamber pressure varied cyclically between 6.7 and 8.0×10^{-3} Pa [air] (S and 6s1 0^{-5} torr) with a period of approximately 9 minutes throughout the test. The reason for this variation is not known. For the conditions of this test the accclc.rater grid current had a sensitivity to tank pressure of 12.7 IitA/l o^{-5} torr as indicated in Fig. 7. This resulted in the cyclic variation in the accelerator grid current shown in Fig. 8. The two sets of data in this figure provide two representative samples of the short term variation in accelerator grid current with time. The average accelerator grid current was determined by integrating under these curves and dividing by the period. The average value clc(cl-mined in this manner was 35 mA.

The high voltage recycle rate as a function of time and the cumulative number of recycles arc given in Fig. 9. These data clearly indicate that for most of the test the recycle rate was considerably higher than that of other long duration tests [Rawlin-1988, Patterson-1990, Brophy-1992]. It is tempting to attribute the high recycle rate to the rapid accelerator grid erosion experienced during this test, but this is by no means a certainty. However, complete penetration of the accelerator grid webbing in the "pits" at the center region of the grid occurred in less than 14S hours of operation. Once penetration of the grid has occurred continued erosion of the accelerator grid can result in the deposition of accelerator grid material on the screen grid. This added material can then cause an increase in the recycle rate by serving as locations for the initiation of grid-to-grid arcing.

Although the recycle rate was very high, the total number of recycles experienced during this relatively short test may be comparable to that experienced by a thruster operated for 10,OOO hours with a "normal" (i.e. much lower) recycle rate. Thus, the effect of recycling (if any) cm the accelerator grid erosion may have been fortuitously accounted for in this accelerated test.

After 14S hours of operation a grid-to-grid short developed The test was stopped and the grids were removed from the thruster body. A substantial number of metallic (s[ccl) flakes were found in the discharge chamber. This material was sputtered from the anode pole piece and resulted from operation at a discharge voltage of 42 to 43 volts. Tantalum foil was spot welded over the anode pole piece assembly and 110 further difficulties with discharge chamber flake formation were encountered in the test, Since it was believed that the grid short was caused by a flake of material from the discharge chamber and not a result of accelerator grid erosion, the short was cleared by blowing compressed dry nitrogen between the grids. This cleared the short without necessitating the disassembly of the accelerator system. This opportunity was also taken to photograph the accelerator grid and to weigh the entire accelerator assembly. These photographs were taken at the center and approximately mid radius and are shown in Fig. 10.

Failure Mechanism

The test was terminated after 633 hours of operation when a permanent grid-to-grid short developed. At this point the thruster was removed from the vacuum system and

partially disassembled. The source of the short was traced to flaking of material sputter-deposited on the screen grid from the accelerator grid which then shorted the grids. The location of this sputter-deposited material was a surprise. Inspection of the accelerator grid revealed a circular trench eroded completely through the accelerator grid at a location approximately 8 mm *outside of'* the outermost ring of holes; a location which is just inside of the ID of the accelerator grid stiffening ring. This trench extended over almost two thirds of the circumference as indicated in Fig. 11 and threatened to sever the accelerator grid from its stiffening ring.

The time at which this trench completely penetrated the accelerator grid is unknown since such penetration could not easily be detected from outside of the vacuum system and since the authors did not know to look for substantial erosion in this location. Once the trench eroded through the grid, further erosion resulted in the deposition of sputtered material on the screen grid. It is this material which subsequently separated from the screen grid and shorted the grids together. An example of sputter-deposited material beginning to flake off from the screen grid at this location is shown in Fig. 12..

Although this flaking phenomena was the failure mechanism for this test, the center region of the accelerator grid was very close to structural failure as will be shown in the following section. Significantly, however, the actual failure mechanism was completely unexpected. It is likely that this failure mechanism is an artifact of operation at the elevated tank pressure used in this test to accelerate the erosion process, although this is not a certainty. A similar groove erosion pattern was noted in a 15,000 hour test performed with mercury propellant at a much lower background pressure, but the total amount of erosion in this groove was considerably less than in the present test. One of the key values in performing a test-to-failure such as the one described in this paper is that it may uncover unknown failure mechanisms. In performing probabilistic failure analyses of the type described in [Polk-1993], neglecting to include a key failure mechanism can lead to potentially disastrous results by giving one an overly optimistic estimation of the thruster reliability.

Post-Test Accelerator Grid Analyses

A closer view of the accelerator grid is given in Fig. 13 and shows that the charge-exchange pits had penetrated the grid out to a radial position within 11 holes of the edge of the active grid area. Close-up, post-test photographs of the accelerator grid are given in Fig. 14. These photographs document the extensive erosion sustained by the grid. At the center region of (1IC grid the charge-exchange pits have grown in the directions along the grooves to the point where only small bridges connect the uneroded regions of the grid webbing and keep the grid from falling apart. The photograph in Fig. 15 shows a location where one of these bridges was eroded through. 011 the side of the grid aperture opposite of this location a substantial amount of grid webbing still exists in the groove indicating a strongly asymmetric erosion pattern around this accelerator grid hole.

The screen and accelerator grids were weighed individually and as an assembly before and after the test and also at run hour 14S (assembly only). The results of these measurements are given in Table 2. These data indicate that the screen grid gained a total of 7.4 g and the accelerator grid lost 42.7 g over the course of the test. The increase in the mass of the screen grid is believed to be the result of the deposition of material sputtered from the accelerator grid by charge-exchange ions. Witness slides positioned near the engine recorded a deposition rate of stainless steel from the vacuum facility of approximately 20 µm/khr. For the total duration of 633 hours this would result in the deposition of approximately 13 µm of stainless steel on the accelerator system. Note that the vast majority of the material deposits are stainless steel even though the target material is carbon (in the form of grafoil). The stainless steel is believed to be sputtered from the sides of the vacuum chamber by divergent beam ions. This stainless steel is removed by the charge-exchange ions in the "pits & grooves" erosion sites, but deposits of stainless steel can be found at the outer radii of the accelerator grid in the regions of the grid webbing surrounding each hole where little erosion takes place. The upper limit for the mass of stainless steel deposited 011 the periphery of the accelerator system is estimated to be no more than 1 or 2 grams. The mass of stainless steel deposited over the active accelerator grid area, but not in the pits & grooves pattern, is estimated to be less than 1 g.

After 145 hours of operation the total accelerator system had lost 8.5 g. Since the photographs in Fig. 10 indicate that the charge-exchange pits had only just begun to penetrate the grid it is believed that there was very little accelerator grid material deposited on the screen grid at this time. Therefore, if we neglect the erosion of the screen grid by the discharge chamber plasma and attribute all of the 8.5 g mass change to erosion of the accelerator grid, then we get a maximum accelerator grid erosion rate of 58.6 g/khr over the first 14S hours. The 42,7 g of accelerator grid erosion experience over the entire test results in an average accelerator grid erosion rate of 67.9 g/khr. Since the accelerator grid voltage and impingement current were constant over the test, this suggests that the material removal rate may be a function of the grid webbing geometry which changes as the grid wears. If this is the case, it suggests that the use of mass loss rates obtained from relatively short term tests will result in an optimistic calculation of accelerator grid life..

The photographs of the upstream side of the accelerator grid given in **Fig. XX** indicate chamfering of the through-pits. This chamfering is presumably created by charge-exchange ions which have passed through the. eroded holes and (hen are attracted back to the accelerator grid. This chamfering of the accelerator grid is not accounted for in the model represented by En. (3), which suggests that the predictions of this model maybe conservative.

Mass 10ss Distribution

The distribution in mass loss as a function of radial position was determined by cutting the grid into 7 concentri ic rings. The electric discharge machining process used to make these cuts has a cut width of approximately 0.3 mm. Each ring was then weighed. The results of these measurements arc given in Table 3. The column labeled "calculated Mass When New" in this table was determined by calculating the grid mass of the grid webbing area when the grid was new based on the measured grid thickness of 360 microns. The thickness of the accelerator grid was measured after the test at the location of the grid covered by the accelerator grid stiffening ring. It is extremely unlikely that any erosion or deposition has taken place at this location. Corrections in the determination of the "new" webbing mass included accounting for the EDM cut widths, and adjustments for the initial non-cylindrical hole shape which is produced by the 50/50 chemical etching process used to form the holes. The mass loss for each ring is then given by the difference between the "Calculated Mass When New" and the measured mass. Dividing these mass loss values by the spherical surface area of each ring gives the mass loss per unit area (g/cm^2) which is plotted in Fig. 16.

The mass loss distribution of Fig. 16 has a flatness parameter (ratio of average to maximum mass loss per unit area) of approximately 0.71. The beam current flatness parameter was not measured for this engine configuration, but it is unlikely that it is a large as 0.71. As mentioned above, the perveance data for the accelerator syste m is consistent with a beam flatness parameter of 0.5S. It is belie\'cd that the flatness parameter for the mass loss distribution may be larger than the beam flatness parameter as a result of operation in a vacuum facility with a non-zero background pressure. Monheiser and Wilbur [Monl~ciscr-1993] suggest that with finite vacuum chamber pressures, charge-exchange ions created far downstream of the engi ne may still reach the accelerator grid. Furthermore, they argue that the fraction of these ions which reach the accelerator grid is a function only of the view factor back to the engine. Even if this model is only qualitatively correct it suggests that charge-exchange ions created neat the centerline of the thruster far downstream of the accelerator grid may strike the accelerator grid at a locations other than near the centerline, thus broadening the radial erosion profile. As a result it is expected that only in space will the mass removal profile be the same as the beam current density profile. Furthermore, this effect implies that ground tests may be misleading to the extent that they can imply a longer g r id life than would actually be achieved in space unless this erosion profile broadening effect is correctly taken into account.

The cumulative mass loss as a function of radial position is given in Fig. 17. This figure indicates that half of the mass loss occurred over the central region of the grid out to a radius of 89 mm. In contrast, for the accelerator grid from the Ref. [Patterson-1990] test half of the grid erosion occurred over the central region out to a radius of 60 mm, and for the test of Ref. [Rawlin-1988] half of the mass loss occurred over the inner 75 mm of the grid [l@!rlin-1993]. These three tests were performed cm three different discharge chambers and with two different propellants so it i s difficult to concretely establish the reason for these differences. Again, it is unlikely that the beam flatness parameter was significantly greater in the present test than for either of the other two tests.

Integrating the. mass loss profile in Fig. 16 results in a total estimated mass ioss from the accelerator grid's pristine condition of 58 g. The mass change determined by direct measurement before and after the test-to-failure was only 42.7 g. Adjusting this mass by approximately 1 g 10 account for the stainless steel deposits outside of the active grid area suggests that the accelerator grid mass change over the 633 hour test should be about 4 4 g. This leaves 14 g unaccounted for (the difference between 58 and 44 g). Most of this difference can probably be attributed to the initial erosion on the grid prior to the test-to-faiiorc. It is unlikely, however, that all of it could be attributed to the initial condition. The integrated mass loss value of 58 g depends on the initial thickness of the accelerator grid, as well as the density of the gr id material. The lack of knowledge of the initial thickness and its uniformity introduces an uncertainty of a few grams in the determination of the integrated mass loss, The grid was fabricated from arc cast molybdenum, so it is likely that the density of molybdenum is c1osc to its maximum value (a quick check of the grid material density was performed and verified this to be the case), Because the test-to-fai]urc test did not begin with an accelerator grid in pristine condition, the integrated mass loss value of 58 g is believed to be a more accurate representation of the mass loss 10 structural failure (starting from a new condition) than the --44 g measured mass change.

Using Eq. (3) to calculate the expected grid mass loss at structural failure results in a value of 63. S g, where the following values were used: r_b = 14?. S mm, t_a = 360 µm, ϕ_a = 0.24, (1 = 0.5, and f_a = 0,71. The value of 0.71 for

the flatness parameter was determined by the mass loss profile in Fig. 16. This is the correct value to use in Eq. (3), but it is something that can't currently be determined a priori for ground based tests. As mentioned above, however, for in-space operation, the beam current flatness parameter should accurately represent the radial mass loss flatness parameter.

Erosion Pattern

The eroded area fraction on the accelerator grid was calculated from measurements taken from photographs of the grid at different locations after 145 and 633 hours of operation. These measurements, given in Table 4, indicate an eroded area fraction of approximately 0.5. Remarkably, these data indicate that the eroded area fraction dots not appear to be a function of radial position or run time as assumed in the model represented by Eq. (3). The difference between the eroded area fraction of 0.50 measured at the center of the grid after 145 hours and the value of 0.48 measured at the same location after 633 hours is an indication of the uncertainty in the procedure used to determine these values.

The eroded area fractions from three other accelerator grids run for extended periods of time are given in Table 5 and compared to that obtained for the test-to-failure. These data indicate no clear correlation of eroded area fraction with any of the parameters listed in the table. The eroded area fraction from the tes(-to-failure is not outside the range of values given by these other tests.

The grid rings described earlier were cut approximately along radial lines in order to measure the thickness of the webbing as a function of radial position. These measurements were made using a scanning electron microscope. At each radial location the maximum grid webbing thicknesses were measured in the eroded and "uneroded" regions of the grid. The maximum grid thickness in the eroded region corresponds to the thickness of the "bridge" which supports the grid near structural failure as identified in Fig. XX. The webbing and bridge thickness measurements as a function of grid diameter are given in Fig. 18. The webbing data suggest a slight thinning of the accelerator grid has occurred at the inner radii, The bridge thickness decreases rapidly as the center of the grid is approached. The difference the bridge thickness and an assumed value for the original accelerator grid Webbing thickness of 360 μm gives the bridge erosion depth which is plotted in Fig. 19 as a function of diameter. The data in Figs. 18 and 19 appear to exhibit more scatter as the center of the grid is approached. This is believed to representative of the actual grid geometry and to an artifact of the measurement technique. A possible explanation for this may be tied to the fact that the center region of the accelerator grid has experienced the greatest mass removal. At this location substantial quantities of molybdenum have been deposited on the accelerator grid. These deposits can form structures which protrude into the screen grid hole as shown in Fig. 21. Such protruding structures can distort the ion beamlet and may result in asymmetric erosion of the bridges.

In the accelerator grid erosion model given by Eq. (3) it is assumed that the erosion pattern remains within the original pits & grooves pattern which is established after relatively short test durations. As the pits erode completely through the grid the ions which used to strike the grid at this location must now strike the grid somewhere else (in order for the accelerator grid current to remain unchanged as seen in Fig. 6). Some of these ion pass through the newly formed holes and get turned around by the electric field between the screen and accelerator grids and strike the accelerator grid on the upstream side forming the chamfers shown in Fig. 14. The chamfers do not, however, represent a substantial amount of erosion compared to the enormous pits which grow in the direction of the bridges. This suggests that after the pits initially wear through the grid the newly formed holes distort the local electric fields sufficiently to result in the re.direction of the charge-exchange ions onto the remaining grid webbing in the grooves. As the pits grow along the grooves in the direction of the bridges, the remaining surface area of grid material in the pits & grooves pattern decreases causing the local ion current density to increase. This suggests that the erosion rate of the bridge should increase as a function of the local amount of grid erosion. That is, when most of the pits & grooves erosion pattern has been eroded though and only a small bridge remains, the rate at which the thickness of tbc bridge decreases should be higher than when the grid was relatively new and no through pits had yet formed. This should be the case even though the accelerator grid current is constant.

The bridge erosion depth data as a function of diameter in Fig. 19 can be used to test this hypothesis. The data of Fig. 19 were all obtained after the same amount of operating time (633 hours), thus a bridge erosion rate could be obtained by simply dividing these data by the run time. This procedure, however, neglects the radial variation in ion current density. This effect can be removed by dividing the bridge erosion depth profile by the mass loss profile from Fig. 16. The resulting quantity represents the fraction of the eroded mass which occurs in the bridge region. Plotting the resulting values as a function of the local mass loss (in g/cm^2) gives the results shown in Fig. 21. If the linear bridge erosion rate were constant with time, then these data should all fall on a horizontal line. That is, a constant linear bridge erosion rate with time, implies that the fraction of the erosion that occurs at the bridge region is constant since the total erosion rate (i.e. ion flux) is constant. Clearly (his is not the case and the data in Fig. 21 indicate that as the grid

wears, a larger and larger fraction of the eroded mass comes from the bridge region.

Beamlet Distortion

The deposition of substantial amounts of material on the screen grid can have adverse effects beyond the potential to produce flakes which can short the grids together as discussed earlier. This material can also project into the Set-cca grid hole as was shown in Fig. 20, and potentially distort the shape of the ion beamlet. The beamlet distortion may be sufficient to result in direct ion impingement on the accelerator grid. Five damaged locations on the accelerator grid (visible in Fig. 13) are believed to be due 10 this effect, Erosion of the accelerator grid webbing by direct ion impingement may result in the formation of a large hole in the grid which, in torn, may impair the grid's ability to prevent electron backstreaming. This failure mechanism could potentially occur before the grid fails structurally.

implications for Accelerator Grid Life

The data from the tcs(-to-failure indicate the time to structural failure of the accelerator grid by charge-cxchangc ion erosion is considerably lcss than calculations based on a linear extrapolation of the bridge erosion rate obtained over relatively short term tests. This is a result of the accelerator grid erosion pattern which remains remarkably unchanged (i.e. within the initial pits & grooves pattern) even when most of the material in the area covered by this pattern has been removed. A mode] based on these experimental observations predicts substantially shorter times to accelerator grid structural failure. '1'here is currently a substantial lack of knowledge of the behavior of the key parameters in this mode], i.e., the eroded area fraction, the radial mass loss profile, and the accelerator grid to beam current ratio for space coalitions. The effect of this lack of knowledge, as well as intrinsic variations in these parameters has been quantified by l'elk, et al. using probabilistic techniques.

The erosion of substantial quantities of accelerator grid material and the formation of relatively large eroded holes in the grid can lead to the deposition of significant amounts of molybdenum on the screen grid. These material deposits may subsequently cause other undesirable effects, such as and increase in grid-to-grid arcing, beamlet distor tion, and flake formatio n which could lead to grid failure. Flaking of accelerator grid material sputter deposited on the screen grid lead to the failure of the IAPS accelerator system tested for 8000 hours [IAI'S].

Conclusions

The following conclusions maybe summarize based on the test-to-failure described in this paper. The first failure mechanism for the accelerator is probably grid shorting due to flaking of accelerator grid material sputter deposited on the screen grid. The second failure mechanism is probably loss of electron backstreaming standoff capability as a result of large grid geometry changes. Possibly due to changes in the beamlet focusing as a result of accelerator grid material sputter deposited on the screen grid, T'bird failure mechanism is probably structural failure. The accelerator grid charge exchange erosion remains largely within the initial pits & grooves erosion pattern even when most of this material is removed. The erosion rate at the location of the "bridges" on the accelerator grid increases with time. Operation at finite vacuum chamber pressures increases the flatness of the accelerator grid mass loss profile relative to that which would be expected in space. Finally, the key parameters in determining the accelerator grid life at a given applied voltage are tllcaccclcrator-to-twain current ratio, the eroded area fraction, and the radial mass loss profile.

Acknowledgments

The authors thank Mr. Vincent Rawlin for providing detailed information regarding the endurance tests performed at NASA LeRC and the data from thruster 11.

The work described in this paper was performed by the Jet Propulsion laboratory, California Institute of Technology, under contract with the National Aeronautics and Space Administration.

References

[Patterson-1993] Patterson, M. J., and Haag, T., "Performance of the 30-cm Lightweight Ion Thruster," IEPC-93-108, presented at the 23rd International Electric Propulsion Conference, Seattle, WA, Sept. 1993.

[Patterson-1990] Patterson, M, J., and Verhey, "I'. R., "5 kW Xenon Ion Thruster Lifetest," AI AA-90-2543, presented at the 21s(Electric Propulsion Conference, Orlando, FL, July 1990 (also NASA TM103191)

[Monheiser-1993] Monheiser, J. M., and Wilbur, P. J., "Effects of Design and Operating Conditions on Accelerator-Grid Impingement Current," IEPC-93-174, presented at the 23rd International Electric Propulsion Conference, Seattle, WA, Sept. 1993.

[Polk-1993] l'elk, J., Moore, N., Newlin, L., aod Brophy, J., "Probabilistic Ion Engine Service Life Assessment," IEPC-93-176, presented at the 23rd international Electric

Propulsion Conference, Seattle, WA, Sept. 1993.

[1 APS]8,0001APStest

[Rawlin-1988] Rawlin, V. K., "Internal Erosion Rates of a 10-kW Xenon Ion Thruster," AI AA-88-291 2, presented at the 24th Joint Propulsion Conference, Boston, MA, July, 1988 (also NASA TM 100954).

[Brophy-1992] Brophy, J. R., Pless, L. C., and Garner, C. E., "Ion Engine Endurance Testing at High Background Pressures," AIAA-92-3205, Presented al the 28th Joint Propulsion Conference, Nashville, TN, July, 1992.

[Rawlin-1993] Personal communication with Mr. Vincent Rawlin, NASA Lewis Research Center, August 1993.

[Nakanishi] Nakanishi, S., "A 15,000-Hour Cyclic Endurance Test of an 8-cm Diameter Mercury Bombardment Ion Thruster," A1AA-76-1022, presented at the International Electric Propulsion Conference, Key Biscayne, FL, November 1976.

'1'able 1 Nominal **Operating Parameter** for the **Test-to-Failure**

Parameter	Value
Beam Current	2,8 A
Screen Grid Voltage	1050 v
Average Accelerator Grid Current	35 mA
Accelerator Grid Voltage	-500 V
Discharge Current	10.8 A
Discharge Voltage	43 V
Coupling Voltage	-20 v
Main Flow Rate	3 s Seem
Cathode Flow Rate	>'sCclll
Neutralizer Flow Rate	5.8 sccm
Tank Pressure Corrected for Krypton	3.5 to 4.1x10^{-3} Pa

Table 2 Grid **Masses**

Date	Accumulated Run Time (hours)	Screen Grid Mass (g)	Accelerator Grid Mass (g)	Total Accelerator System Mass (g)
10123/92	0	1725.1	702.5	2428.4
12/9/92	145	-----	-----	2419.9
1/1 5/93	633	1732.5	659.8	2392.8
Net Change	------	+7.4	-42.7	-35.6

']'able 3 **Accelerator** Grid Mass **Loss Distribution**

Ring Number	1 nncr Radius mm)	Outer Radius (mm)	Mass after 633 hours (g)	Calculated Mass When Ncw (g)	Estimated Mass Loss Per Unit Area (g/cm^2)
1	0	12.7	0.6939	1.44	0.155
2	13.0	38.1	5.8422	11.54	0.147
3	38.4	63.5	11.8252	23.08	0.146
4	63.8	88.9	18.844	35.56	0.138
5	89.2	114.3	28.55	45.17	0.118
6	114.6	139.4	43.8	57.04	0.080
7	139.7	N/A*	548.2		N/A

*Includes accelerator grid stiffening ring.

Table 4 Eroded Area Fraction for the Test-to-Failure

Location	Total Run Time (hours)	Eroded Area Fraction a
Center	145	0.50
Center	633	0.48
Mid-radius	633	0.50
Edge	633	0.49

Table 5 Comparison of 2-Grid, Long Duration Tests

Parameter	Test-to-Failure	NSTAR 900-hr Test at 5.5 kW Ref. [XX]	NSTAR 500-hr Test at 10 kW Ref. [YY]	Thruster J1
Propellant	Kr	Xe	Hg, Xe	Hg, Xe
Tank Pressure (Pa)	3.5104.1 x 10^{-3}	1.7X 10^{-3}	1.9x 10^{-3} (Xe)	8.7 x 10^{-5} (Hg)
Accel. Grid Voltage (V)	-500	-330	-500	-308
Accel. Grid Current (mA)	..	17.4	47	5
Duration (hrs)	633	960	567 (Xe) 5300 (Hg)	-6200 (Hg) -200 (xc)
Accel. Grid Hole Dia. (mm)	1.14	1.14	1.s2	1.14
Center-to-Center Hole Spacing (mm)	2.21	2.21	2.21	2.;21
Eroded Area Fraction	0.50	0.40	0.s4	0.46

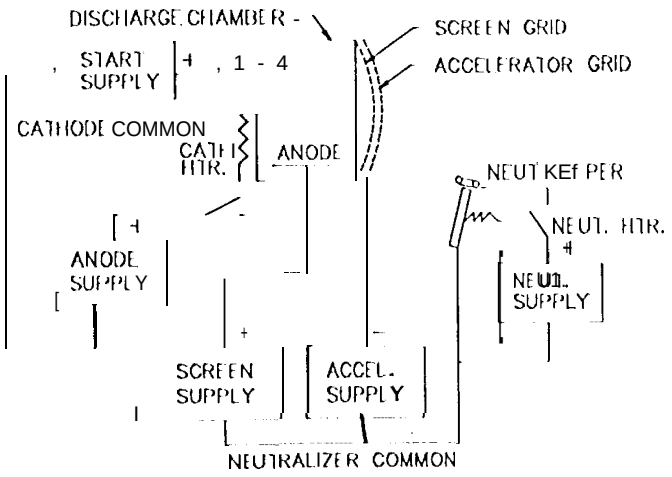

Fig. 1 Power supply block diagram.

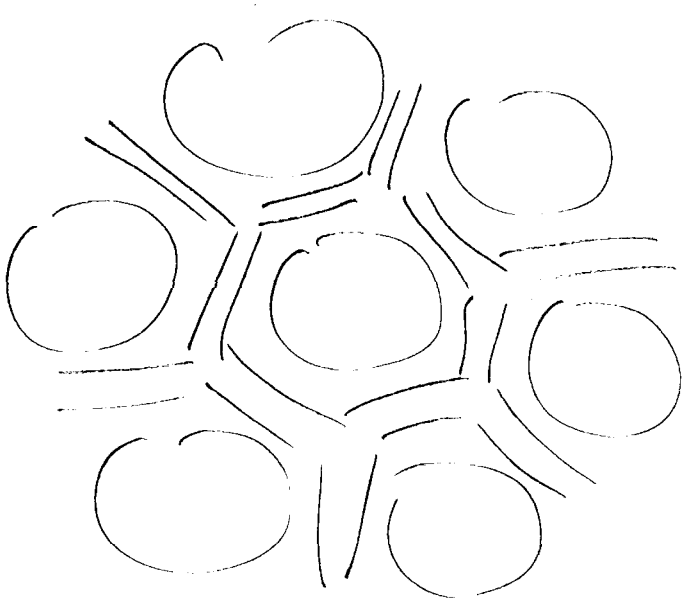

Fig. 2 "Pits + Grooves" erosion pattern

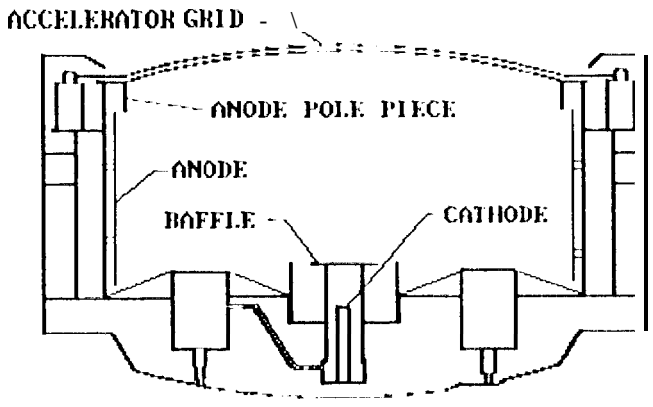

J-Series

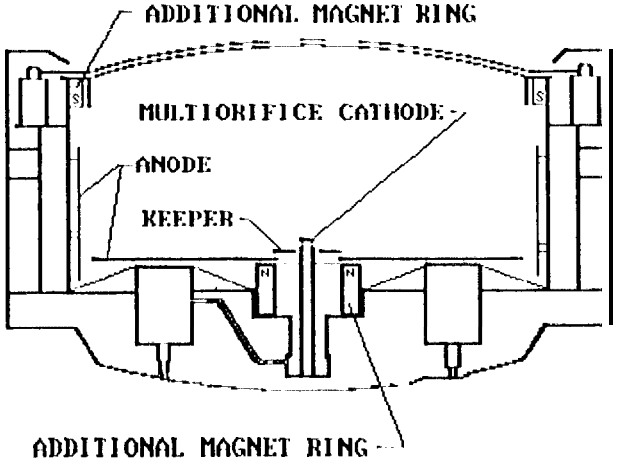

As modified

Fig 3 Ion engine configuration comparison.

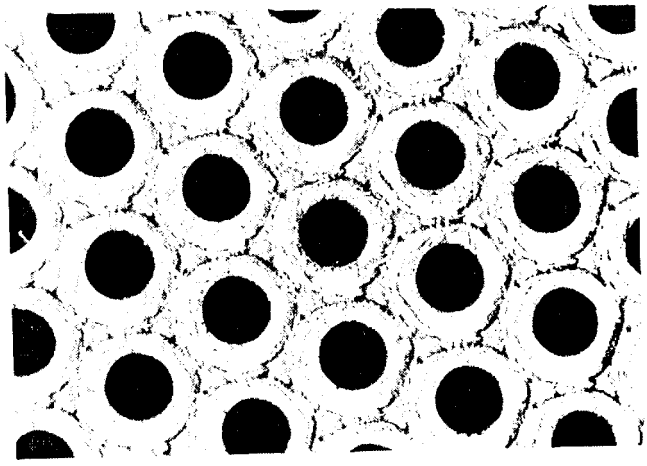

Center

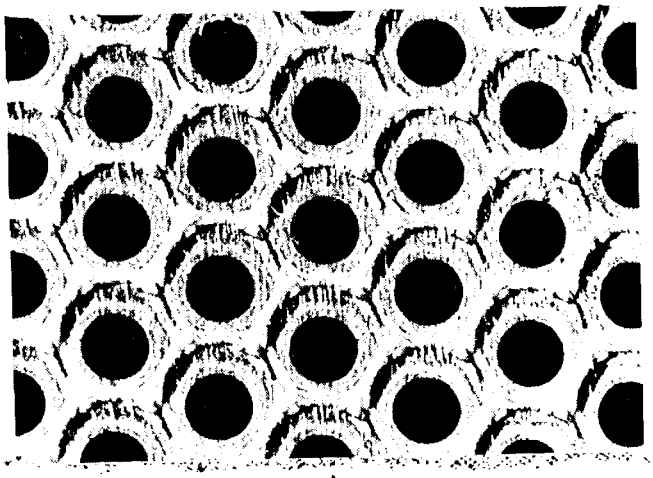

Mid-radius

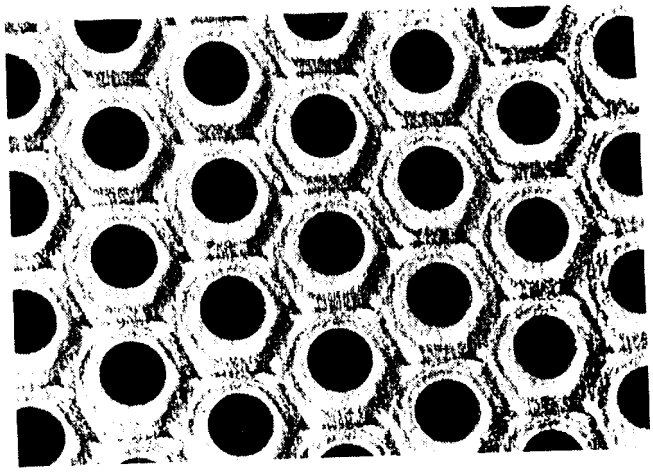

Edge.

Fig. 4 Initial accelerator grid downstream ion surface. condition.

1/9/93

Fig 3

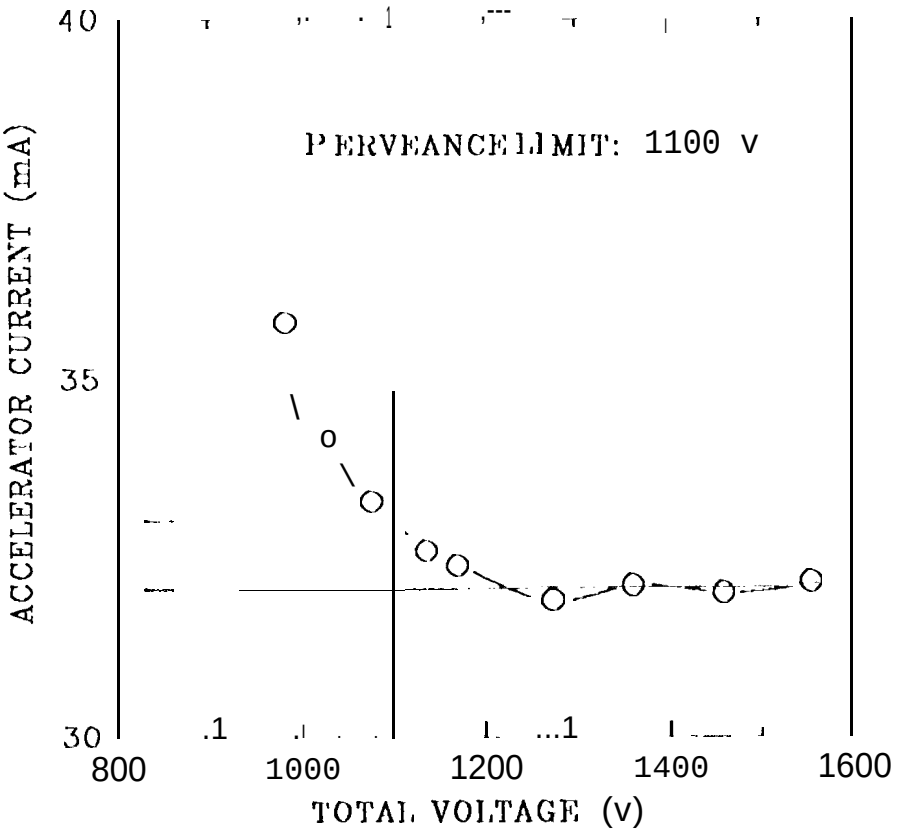

Fig. 5 Perveance determination for a Kr beam current of 2.8 A.

Fig. #6

Test to failure operating characteristics

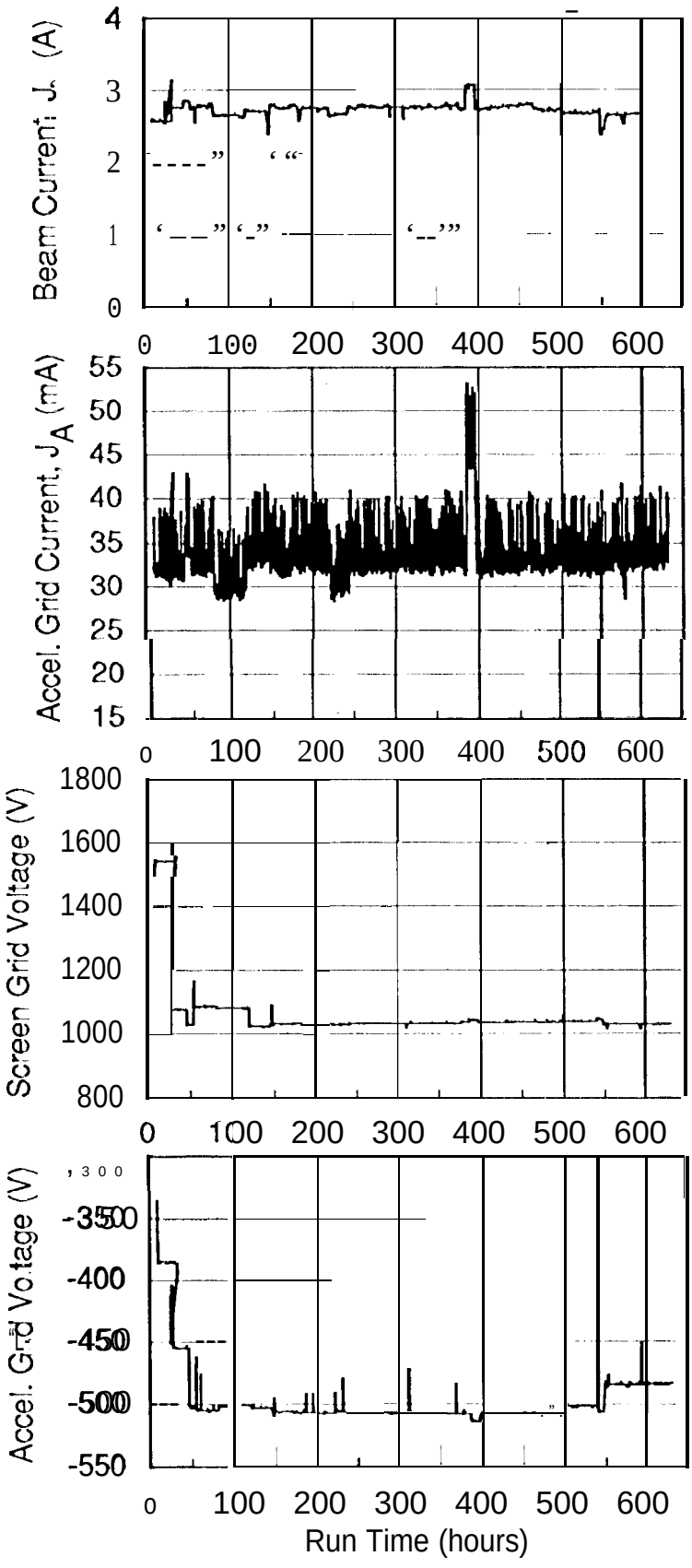

Fig. 6. Test to failure operating conditions

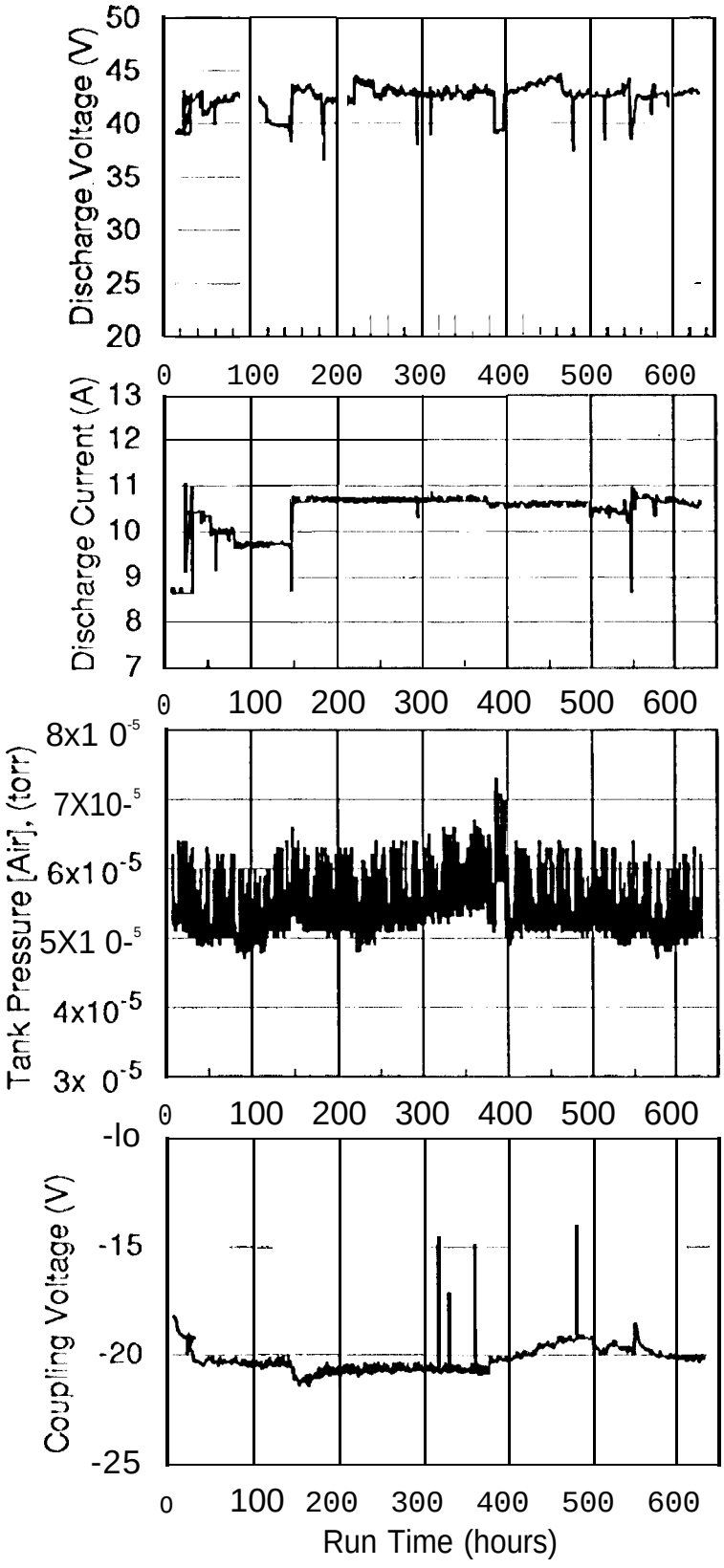

* Uncorrected for Kf.

Fig. 6 continued

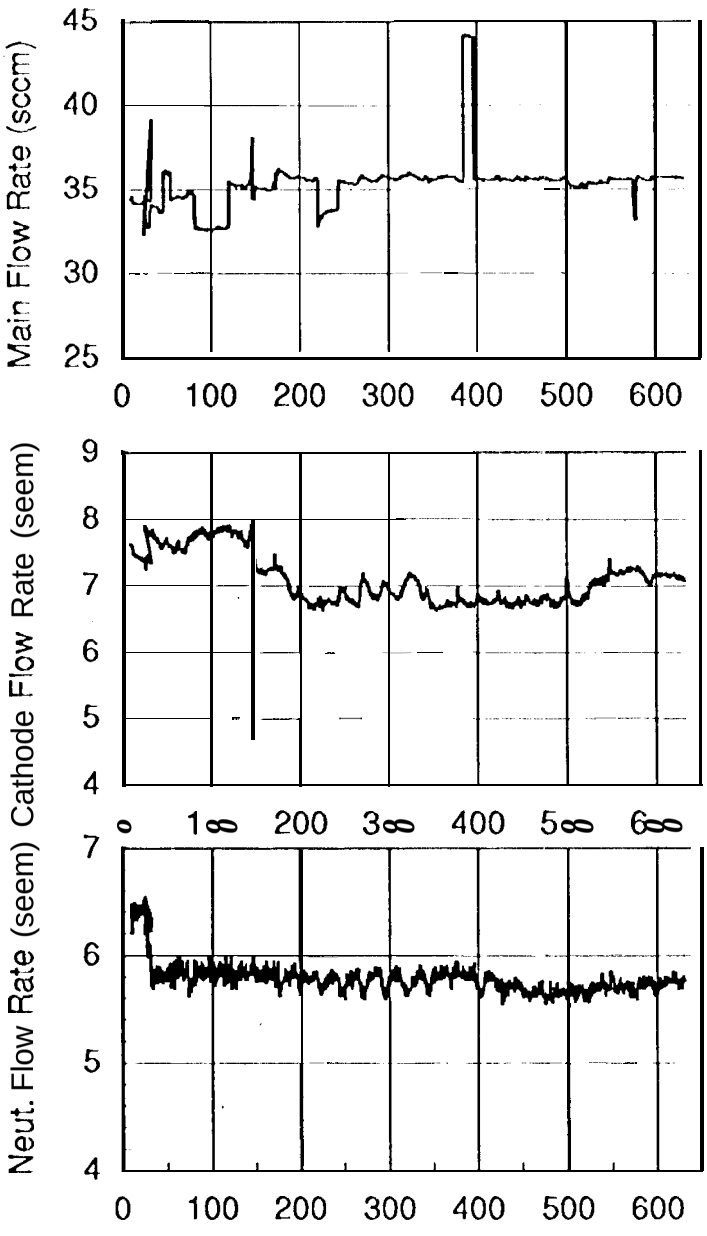

Fig. 6 Concluded

1/22/93
= TIPRES.SPS

Fig 4 & 7

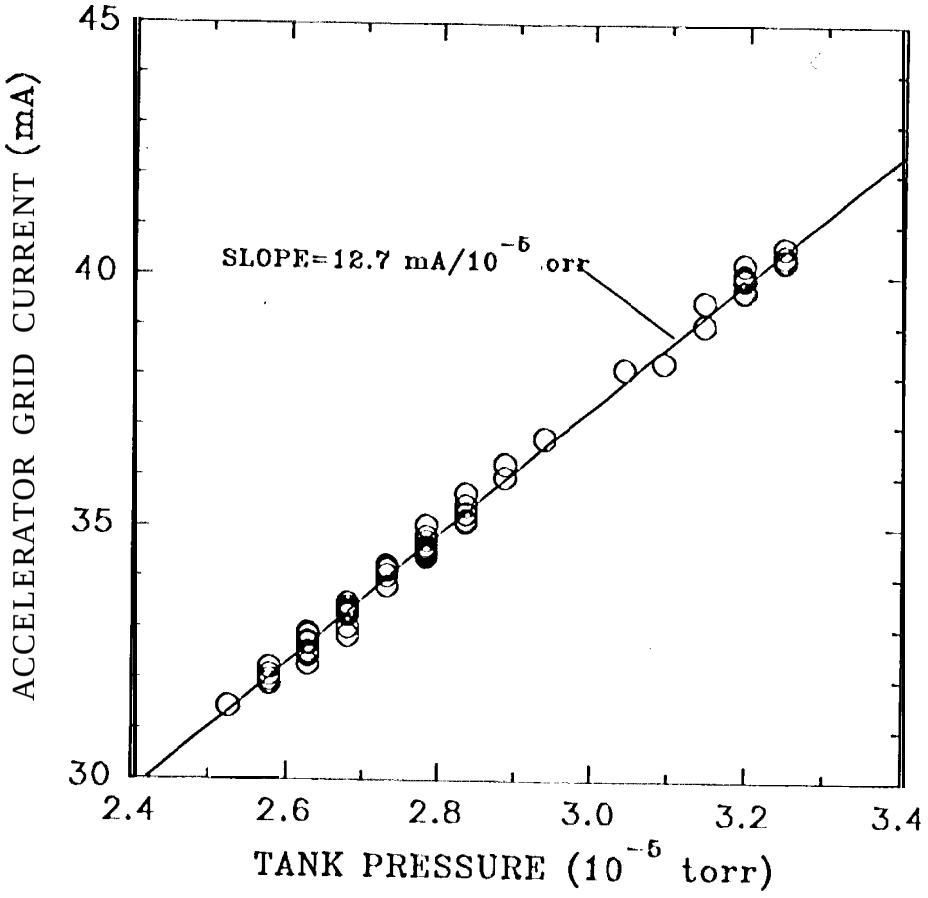

Fig. 7 Accelerator Grid current sensitivity to tank pressure.

1/9/93

Fig. 6 8

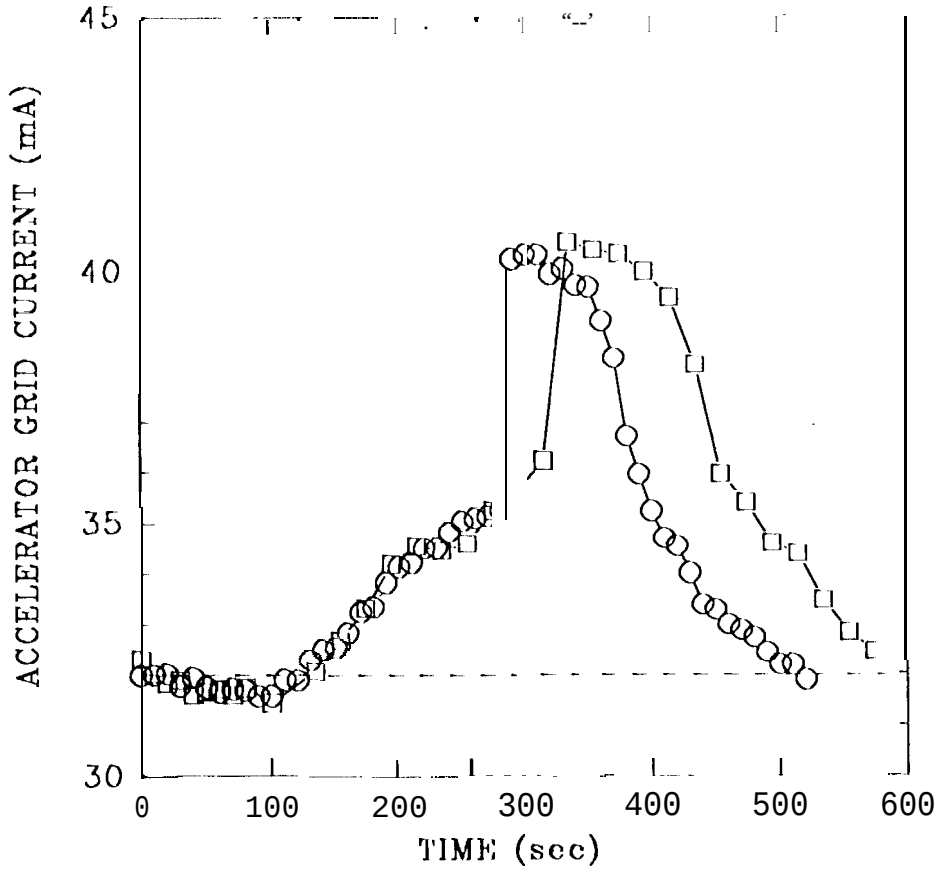

Fig 8 Accelerator grid current variation with time (short time scale).

Fig. 9

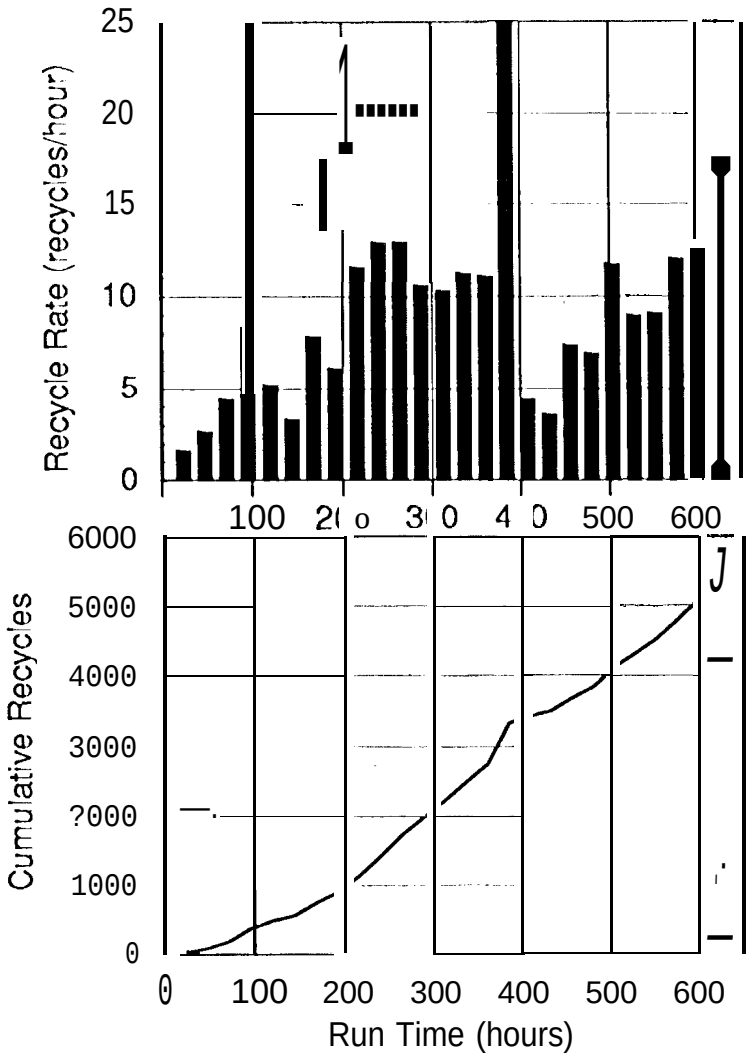

Fig. 9 High voltage recycle characteristics during the test-to-failure.

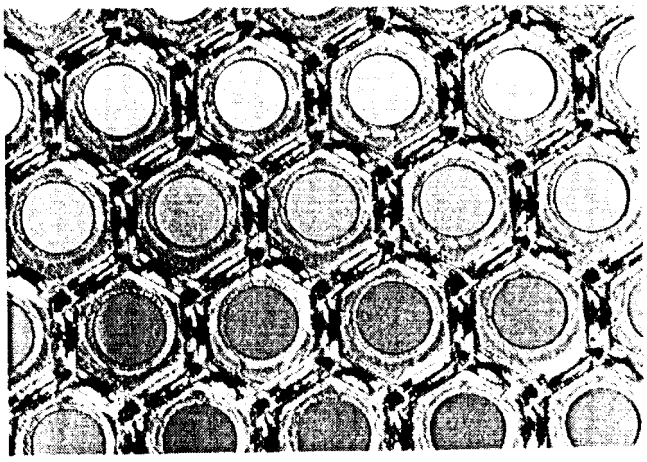

Ended

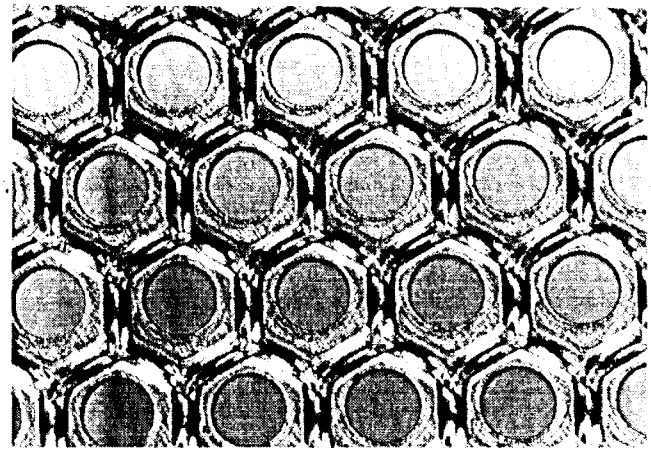

Mid-radius

Fig. 10 ~~A~~ Downstream accelerator grid surface after 145 hours

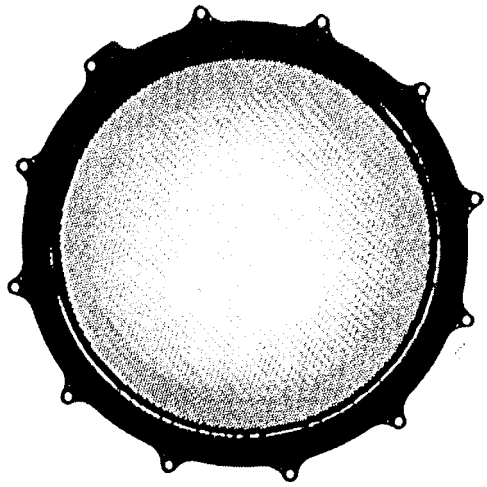

Fig. 11 Post test condition of the accelerator grid showing eroded trench outsi of the hole pattern extending from 2 o'clock to 9 o'clock

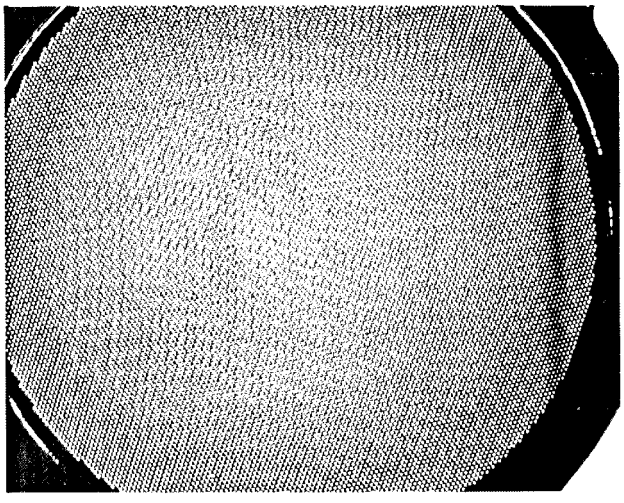

Fig. 12 Closer view of accelerator grid. Damaged regions of the grid are visible.

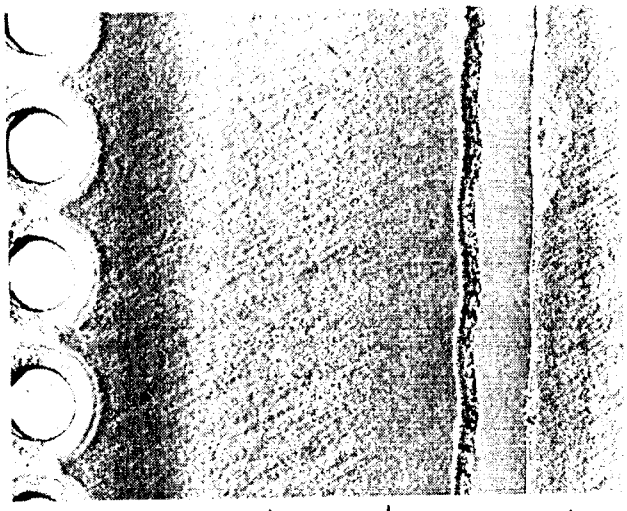

Accel. grid, upstream side.

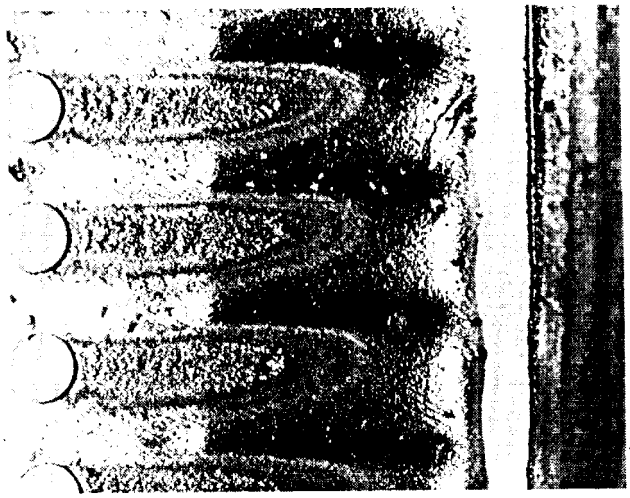

Accel. grid, downstream side.

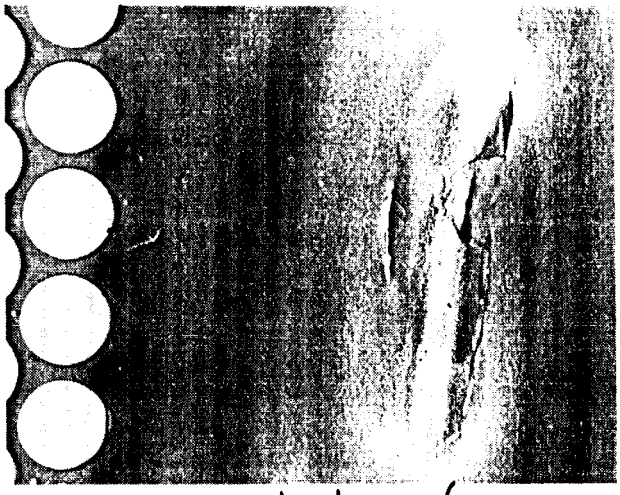

screen grid, deposits on the accelerator grid

Fig. 13 Trench erosion and material deposition on the screen grid

Upstream side

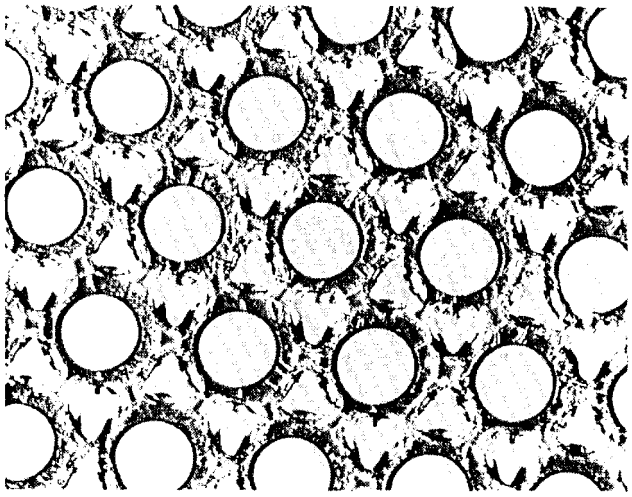

Center

Downstream side

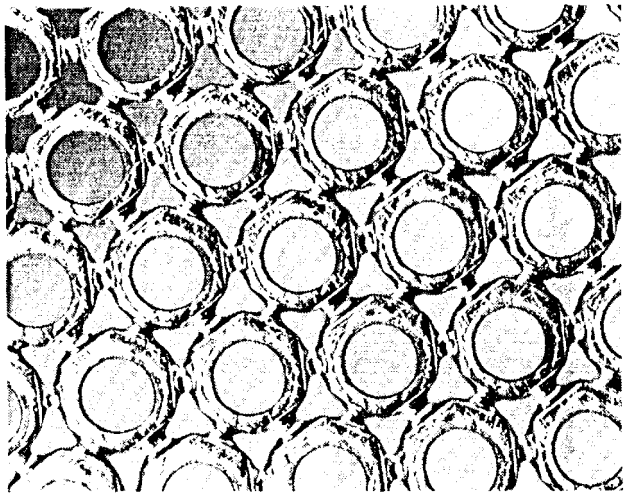

Center

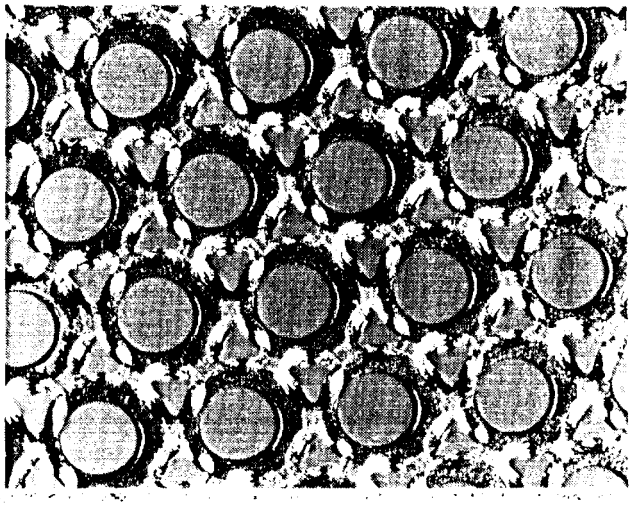

Mid-radius

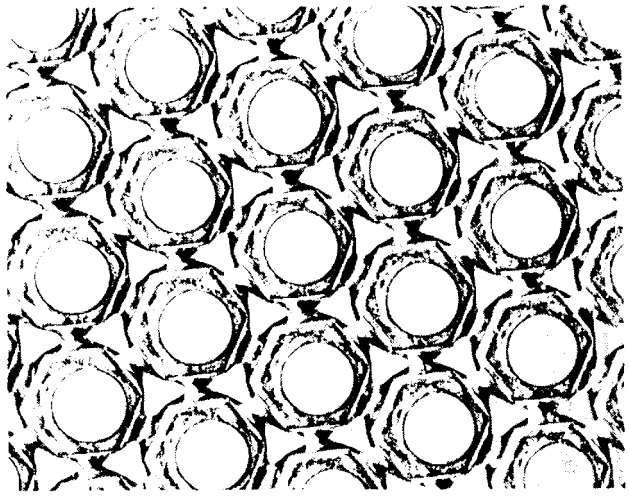

mid-radius

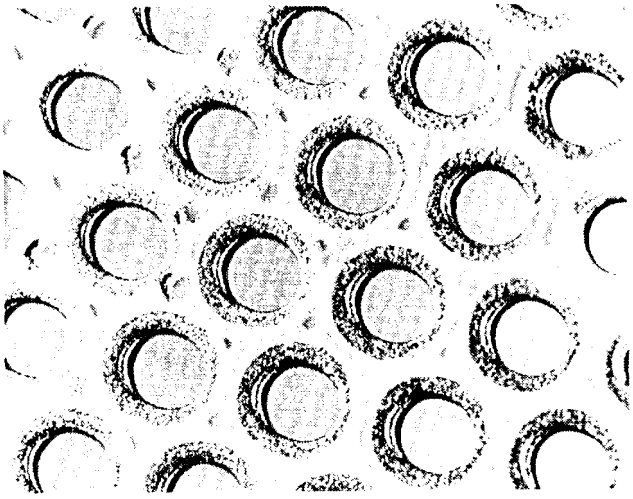

11 holes from edge

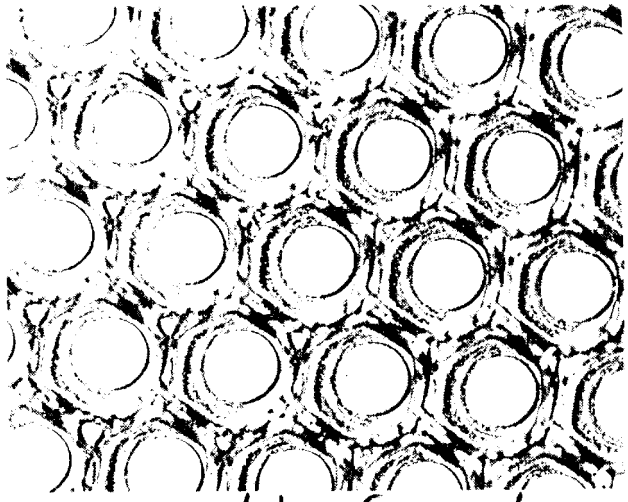

11 holes from edge

Fig. 14 Accel. grid post test conditions

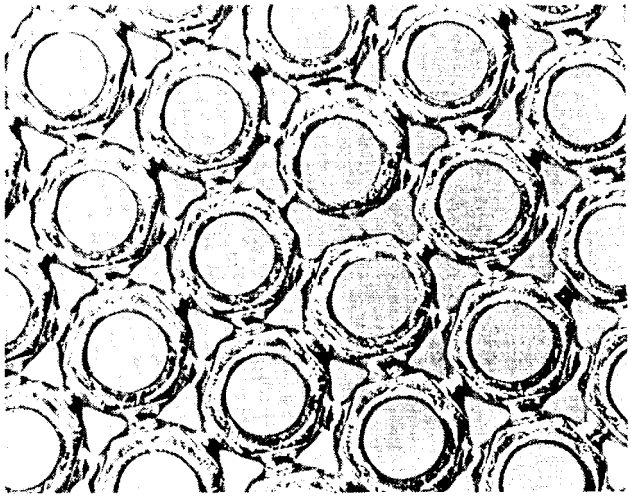

Fig. 15 Broken webbing on accelerator grid

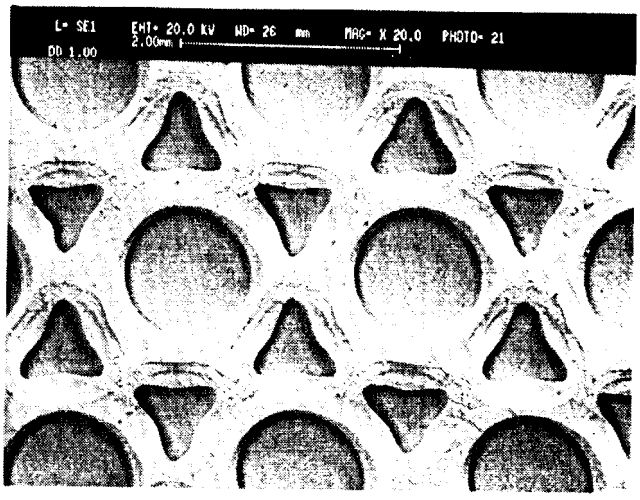

Fig. 15a SEM of upstream side of the accelerator grid.

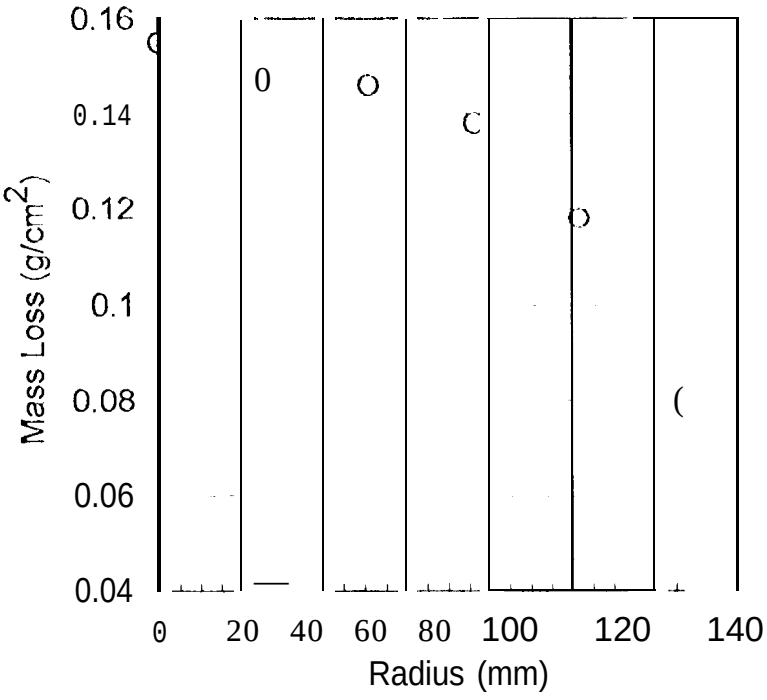

Accelerator grid

Fig. 16 Radial mass loss profile

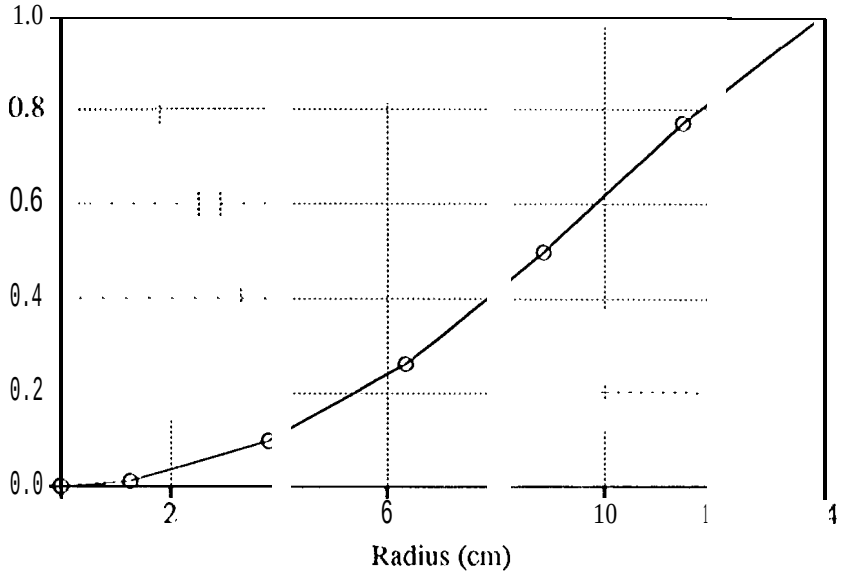

Fig. 17 Accelerator grid cumulative mass loss profile

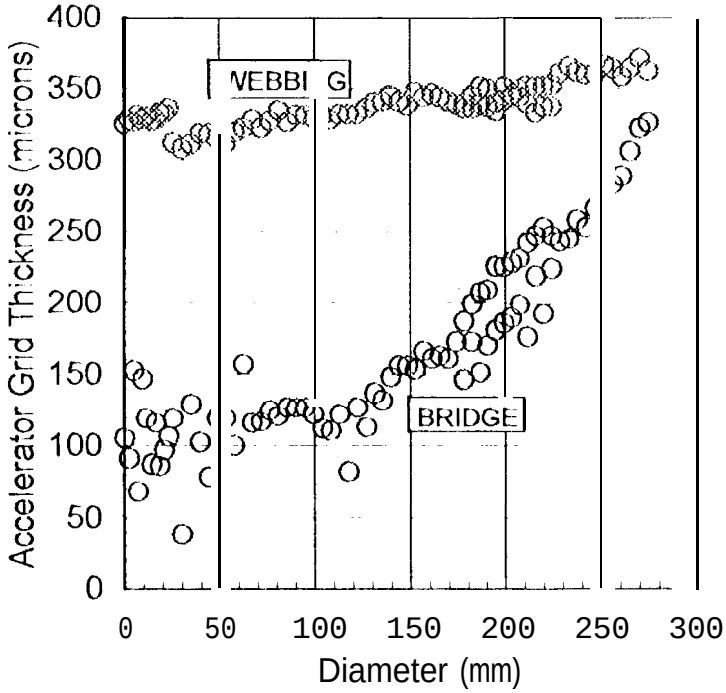

Post test-to-failure

Fig. 18 "Measured" accelerator grid bridge and "uneroded" webbing thicknesses

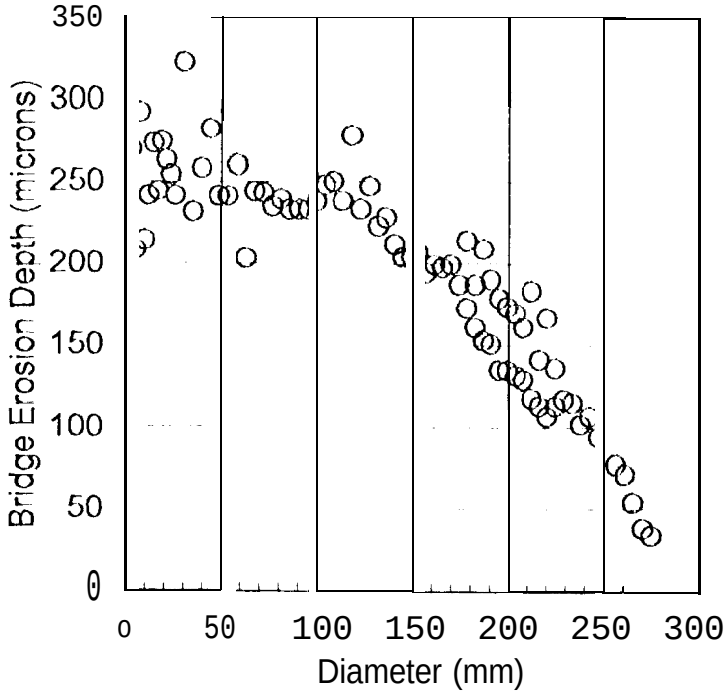

Fig. 19 Bridge erosion depth assuming an initial grid thickness of 360 μm.

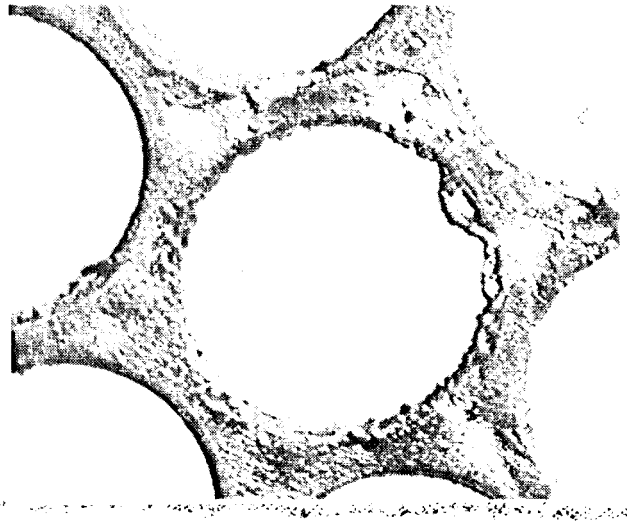

Fig. 20 Material sputter deposited on the downstream side of the screen grid from the accelerator grid

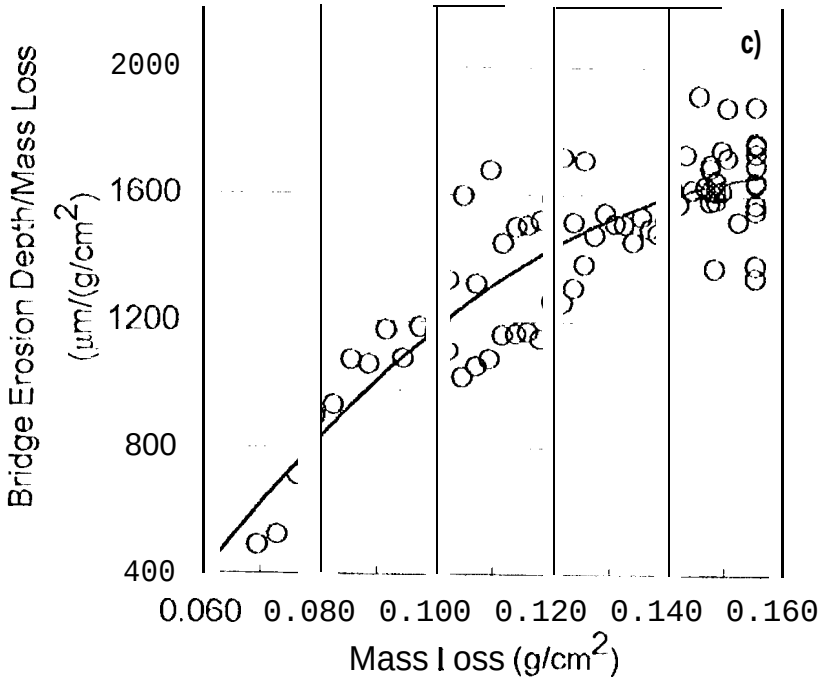

Fig. ~~22~~ 21 The vertical axis represents the fraction of the local mass erosion that occurs at the bridge region. This fraction increase ~~to~~ with the quantity of ~~mass~~ the local mass removed.

$\frac{g}{cm^2} \cdot \rho d = \frac{g}{cm^3} \cdot cm$

$\rho d =$